Journal of
Materials Chemistry B

Accepted Manuscript

This article can be cited before page numbers have been issued, to do this please use: B. Roondhe and P. K. Jha, *J. Mater. Chem. B*, 2018, DOI: 10.1039/C8TB01649F.

ROYAL SOCIETY OF CHEMISTRY

rsc.li/materials-b

View Article Online
DOI: 10.1039/C8TB01649F

Journal Name

ARTICLE

"Haeckelite" a new low dimensional cousin of boron nitride for Biosensing with ultra-fast recovery time: A first principles investigation

Received 00th January 20xx,
Accepted 00th January 20xx

DOI: 10.1039/x0xx00000x

www.rsc.org/

Basant Roondhe [a] and Prafulla K Jha*[a]

We performed state of art first principles calculations under the frame work of dispersion corrected density functional theory to investigate the electronic and vibrational properties of recently found allotrope of BN with octagonal and square ring forming planar haeckelite structures (haeck-BN). We further investigated the adsorption mechanism of five nucleobases adenine (A), guanine (G), cytosine (C), thymine (T) and uracil (U) over haeck-BN to explore its applicability in biosensor. The dispersion correction (DFT-D2) is included to consider the proper account of van der Waals interaction. The order of the adsorption energy of nucleobases over haeck-BN has the following order: G > T > A ≈ C > U. Significant variation in the electronic properties, density of states and work function confirm the adsorption of nucleobases. To check the reusability of haeck-BN as a biosensor toward nucleobases, we have calculated the recovery time. Ultrafast recovery time (in millisecond) viz., 292 ms, 130ms, 120ms, 160ms and 0.6ms is predicted for G, A, C, T and U respectively. Our finding suggests that haeck-BN can be utilized as a biosensor for the detection of nucleobases due to its superiority from graphene, h-BN and boron nitride nanotubes and can be further explore for photocatalyst.

1. Introduction

The last decades were totally dedicated to study the wide range of carbon-based materials. Due to the remarkable properties of new carbon forms such as fullerenes, carbon nanotubes and graphene, much interest has been developed among the scientific community for their use in several technological areas.[1–4] Among all carbon forms, graphene has attracted great research interest since its successful fabrication in 2004.[4] Graphene has a symmetrical hexagonal honeycomb atomic structure resulting into its extraordinary and excellent physical properties.[5–10] From the wide investigation of this outstanding material it has been explored as a promising material for spin and nano electronics.[11,12] The discovery of graphene motivated the researchers to explore other 2D materials as graphene confirmed the existence of 2D material. So far, monolayers of h-boron nitride (h-BN), silicon, transition metal sulfide, phosphorous and many others have been synthesized or predicted.[13–21] A significant impact for the development of nanodevices and nanoelectronics has been gathered by these 2D materials due to their astonishing electrical, optical, and mechanical properties.[5–12] As 2D materials which are having traditionally hexagonal structure has gathered attention because of the impact of the structure on various properties of material. This is because in any material the properties are associated with the position of the atoms in the structure and can answer the formation of electronic structure in the material. BN nanostructures being isomorphic to carbon have been extensively explored for their immense chemical and thermal stability by virtue of their exceptional properties.[22,23] Owing to the geometrical similarity, h-BN sheet which is an insulator with large bandgap in contrast to semimetal graphene possesses many excellent properties similar to graphene like good thermal conductivity, strong mechanical properties and high thermal stability.[24,25] Graphene has a non-polar C-C bonding whereas B-N bond is highly polar in h-BN sheet.[26,27] Due to the unique properties, h-BN sheet has applications in lubricants, dielectric material, as insulator in electronic devices etc..[28,29]

The existence of new form of structure in 2D material was demonstrated based on the presence of square-octagonal pair in BN monolayer grown on Cu (111) surface[30] as defect states of h-BN. This formation of square-octagonal pair in h-BN was also predicted by Liu et al..[31] Following these studies, a periodic structure consisting of square-octagonal pairs of GaN[32] and ZnO[33] were theoretically predicted and studied. However, the possibility of similar periodic structure with repeating square-octagonal pairs of Boron and Nitrogen were not considered yet to the best of our knowledge even though the existence of square-octagonal units of h-BN was proven experimentally. Thus, motivated by the experimental work of

[a] Department of Physics, Faculty of Science, The Maharaja Sayajirao University of Baroda, Vadodara-390002, India.
*Email:prafullaj@yahoo.com; pk.jha-phy@msubaroda.ac.in

Electronic Supplementary Information (ESI) available: [Supplementary material contains Charge density plots, HOMO-LUMO, Partial density of states (PDOS) and work function plots of nucleobases adsorbed haeck-BN system]. See DOI: 10.1039/x0xx00000x

View Article Online
DOI: 10.1039/C8TB01649F

Li et al. and theoretical studies of haeckelite GaN and ZnO, we performed the first principles calculation of haeckelite-BN

Deoxyribonucleic acid (DNA) and Ribonucleic acid (RNA) are in the main focus of researchers from the past few decades as they are the key component of genome and the centre of biological system. The basic building block of nucleotide is nucleobase which carries all the information of the DNA, having purine as its base compound. Many studies have been reported which provide a brief description of sensing phenomena of nanostructures with nucleobases.[34–40] There are few advantages of h-BN over graphene such as h-BN is less hydrophobic which minimizes its hydrophobic interaction with DNA to avoid its translocation, thickness compared to the nucleotide spacing in single strand DNA[41] and unchanged fundamental properties of both h-BN and DNA are important parameter for DNA research.[42] Zhi et al.[36] have reported a strong interaction between the BN nanostructures and the nucleobases compared to graphene, due to the presence of dissimilar atoms. The cytocompatibility of boron nitride nanostructure (BNNs) with living cell has also been reported.[37,38] Liu et al.[39]and Zhang and Wang[40] have reported the genome and DNA sequencing using BN nanopores. Jin et al.[43] explored MoS_2 as bio sensor and reported improvement in the sensing of nucleobases by modifying its surface with Au. All these studies have enhanced our understanding about the utilization of BNNs in nano-biomedical application.[44,45]

Motivated with the success of BNNs in sensing and detecting the biomolecules, we contemplated to explore this new form haeck-BNNs i.e. haeckelite boron nitride nanostructure as a possible biosensor. The different interatomic distance and bond angles in haeckelite two dimensional structures compared to usual two dimensional structures arising due to an octagonal and square ring is expected to interact differently with the adsorbates similar to the porous material. Furthermore, a different kind of interaction between adsorbate and haeck-BN is foreseen because of the presence of all atoms in haeck-BN unit cell. To the best of our knowledge, 2D haeckelite monolayer structure of BN has not been explored theoretically for biosensing applications. In the present work we aim to investigate the structural, electronic and phonon properties of haeck-BN. While electronic properties of haeck-BN show possibility of its use in electronic devices, the phonon properties will be of use to understand its thermal properties apart from its prominent dynamical stability. Finally, we understand the adsorption mechanism of the nucleobases over its surface. The study of structural geometries, electronic properties, phonon dispersion of haeck-BN, adsorption and charge transfer of haeck-BN functionalized by Adenine (A), Thymine (T), Guanine (G), Cytosine (C) and Uracil (U) nucleobases are done. The state-of-the-art ab-initio calculations are used to uncover the dispersion effect on the interaction of nucleobases with haeck-BN. Thus, this study will be unrevealing the nature of interaction of nucleobases with haeck-BN to get atomic level understanding about these hybrid systems for various applications.[46,47]

The paper is organized as follows: The computational details are given in Section 2. The structural and electronic properties of the haeck-BN monolayer are described in Section 3.1. The phonon dispersion of haeck-BN monolayer is discussed in Section 3.2. The adsorption mechanisms are described in Section 3.3. Finally, the conclusion is in the last Section 4.

2. Computational Methods

All calculations were performed using first principle calculation under the frame work of density functional theory (DFT) implemented in Quantum Espresso code[48] which uses plane-wave basis sets to expand Kohn-Sham orbital. The Broyden-Fletcher-Goldfarb-Shanno (BFGS)[49] method was used for the ground state optimization of all structures. The generalized gradient approximation (GGA) proposed by Perdew-Burke-Ernzerhof (PBE) was employed to treat exchange-correlation functional in ultrasoft pseudo potential.[50] The plane wave basis set with 80 Ry and 800 Ry cut off energy and charge density respectively was used for single particle functions which were sufficient to fully converge the lattice parameter and total energy. The Brillouin zone (BZ) integration was performed within Monkhorst-Pack[51] scheme with k-mesh 16 x 16 x 1 for the unit cell and 8 x 4 x 1 for the (2 x 3) supercell (the convergence plots of kinetic energy cutoff and number of k-points are provided in the supplementary Figure S1). These k–points mesh guarantee a violation of charge neutrality less than 0.009e indicating adequate convergence of the calculations. The iterative Davidson type diagonalization method was used to solve the Kohn – Sham equation with energy convergence threshold of 1×10^{-8} Ry. The density functional perturbation theory (DFPT) implemented in Quantum Espresso code[52] was used to compute the phonon properties which allows the calculation of phonons at any wave vector in the unit cell. The q mesh of 10 x 10 x 1 is used to calculate dynamical matrix for 2D monolayer of haeck-BN by applying acoustic sum rule for $q \rightarrow 0$. The dynamical stability was also ensure by the phonon frequencies calculation along the whole Brillouin Zone (BZ) which is computed by the forces obtained after the perturbation method in quantum espresso package. Comparative analysis has been carried out to understand the interaction of haeck-BN with five nucleobases by structural optimization, adsorption energy calculation and density of states (DOS) plots. Accounting of the dispersion forces has been emphasized in the literature which is a precise quantum mechanical description which explains the interaction of molecule with nano-surface[53], therefore for the description of long-range electron correlation it is important to choose a suitable computational method. The present study employed the Grimme's dispersion correction[54] to consider the long range van der Waals interaction (i.e. ~ 3 Å) between the nucleobases and the haeck-BN monolayer. The adsorption energy E_{ad} has been calculated according to the following equation

$$E_{ad} = E_{(haeck-BN+nucleobase)} - \{E_{(haeck-BN)} + E_{(nucleobase)}\} \quad (1)$$

where, $E_{(haeck\text{-}BN\ +\ nucleobase)}$ is the total energy of haeck-BN adsorbed by nucleobase (Adenine (A), Thymine (T), Guanine (G), Cytosine (C) and Uracil (U)), $E_{(haeck\text{-}BN)}$ is the total energy of the adsorbent haeck-BN monolayer, $E_{(nucleobase)}$ is the total

View Article Online
DOI: 10.1039/C8TB01649F

energy of nucleobase (A, T, G, C and U) obtained from their full optimized geometries.

3. Result and Discussion

3.1 Structural and electronic properties

To understand the structural and electronic properties of any system, the system should be fully relaxed and optimized. We have first optimized the geometry and related parameters of the primitive cell of the haeck-BN monolayer structure by calculating the lattice constant and ground state energy. The optimized structure of the haeck-BN monolayer is shown in Fig.1 (a). From figure it is clear that the primitive cell which has tetragonal P4/mbm (127) space group is different from bulk h-BN as well as 2D h-BN shown in Fig.1 (b-c). While the bulk BN has $P6_3/mmc$ (194), $P6_3mc$ (186) and $F4\bar{3}m$ (216) space groups respectively for bulk h-BN, wurtzite BN and zinc blende BN[55,56], the 2D h-BN have hexagonal honeycomb lattice with P-62m (189) space group. The haeck-BN unit cell has entire atom situated in the center part but not at the corner. The Haeckelite structure has octagonal and square ring which give different interatomic distances and bond angles. The bond distance d of B-N is 1.402 Å for bond in square ring and 1.475 Å for bond in octagonal ring. The calculated bond angles in the square ring are 84.21° and 95.78°, while in the octagonal ring the bond angles are 132.10° and 137.11°. The bond length of B-N in haeck-BN is significantly different from the bulk BN as well as 2D h-BN as the bond length between B-N varies from 1.45 to 1.568 Å.[55] The bond length of B-N in haeck-BN is 0.045 Å less in square ring as compared to h-BN and the bond length between B-N at octagonal ring is 0.025 Å large. This is the major structural difference between both monolayers; h-BN and haeck-BN. The optimized lattice parameter along with calculated bond angles and bond length are presented in Table 1.

Table 1 Table 1 Calculated Lattice a (Å), Bond length (Å), Bond angle (°), Energy band gap Eg (eV), Fermi level energies EF(eV).

System	Lattice a (Å)	Bond angle (°)	Bond length (Å)	E_F(eV)	E_g(eV)
BN-Haeckelite	4.929	84.21 and 95.78 (for square ring)	1.402 (bond in square ring)	-2.332	3.91
		132.10 and 137.11 (for octagonal ring)	1.475 (bond in octagonal ring)		

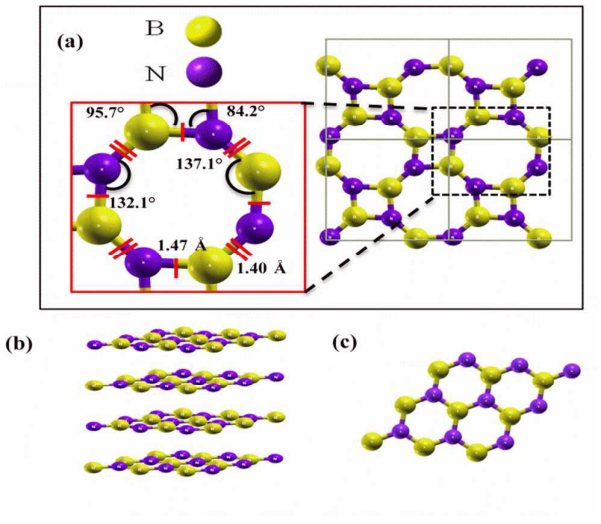

Fig. 1 (a) Optimized structure of haeck-BN monolayer in addition with the enlarge view having bond length and bond angle, (b-c) Structure of bulk h-BN and 2D h-BN. Yellow and purple ball represents boron and nitrogen respectively.

As known that the electronic band structure is the key to understand the electronic properties of any material, we have further calculated the band structure of haeck-BN. One of the important information about the masses of the electron can also be found from the band dispersion. The calculated band structure for haeck-BN along **k** path **Γ–M–X–Γ** of the Brillouin Zone (BZ) is shown in Fig. 2 along with the density of state and orbital contribution as PDOS. The highly dispersive bands in the conduction band region suggest small effective mass for electron. A direct band gap of 3.9 eV is observed between **Γ-M** which is lower than the bulk h-BN, z-BN and w-BN which have large indirect band gap of 4.47 eV, 5.72 eV and 4.50eV respectively.[55] The significantly lower and direct bandgap in h-BN makes it an interesting material to be explored for optoelectronics and biosensors.[57] The boron and nitrogen atoms take equal part to form the electronic band structure of haeck-BN. The right panel of Fig. 2 presents the total and partial density of state of haeck-BN for proper understanding of electronic contribution. From the figure we can see that the boron atoms have a dominating contribution in the conduction band (between 2 - 6 eV) with its p_x orbitals while p_y and p_z have little contribution in the valence band (between -4 to -8 eV). The nitrogen atom contributed majorly in the valence band region with its p_x orbital electron between -2 to -4 eV and p_y and p_z contributed in the lower valence band region between -4 to -8 eV. But in case of bulk BN the valence band maxima mainly comprise of N-p_z and conduction band has B-p_z orbitals contribution.[55]

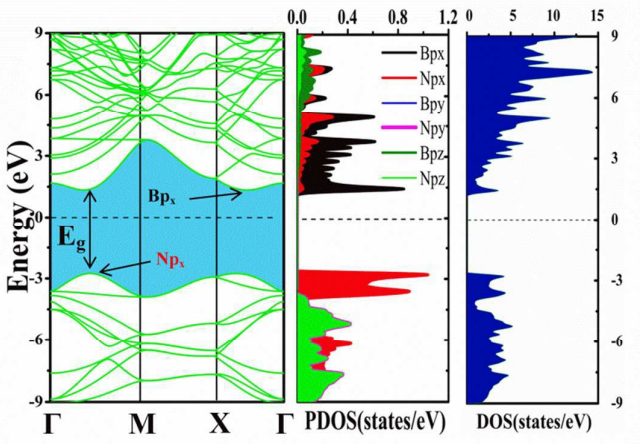

Fig. 2 Calculated band dispersion curve of haeck-BN. Along with total DOS and PDOS of haeck-BN at the right panel.

In order to predict the chemical bonding and the charge transfer in haeck-BN, the charge-density behaviors are

View Article Online
DOI: 10.1039/C8TB01649F

calculated in the (110) plane for this compound and is depicted in Fig. 3. Electronegativity values for B and N are +0.1196 and

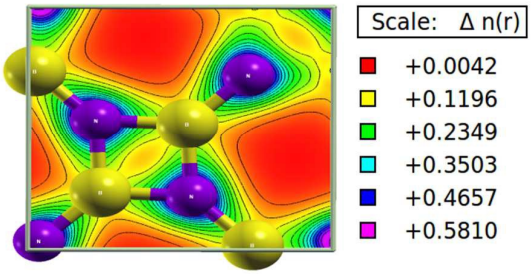

Fig. 3 Total charge density plot of haeck-BN. The blue colour represents the large value of electron charge density while red colour shows relatively low charge density

+0.4657 respectively. The plot shows covalent bonding between B and N atoms in haeck-BN. The iso-density plot shows no vacancy as density is evenly distributed throughout. The charge between B and N is shared by covalent bond between them. The maximum charge accumulation sight is near nitrogen atom (blue color; +0.4657), which shows the localization of electron around it.

3.2 Vibrational Properties

Phonon dispersion calculations are the key to understand the dynamical stability of any material as it provides an insight to the mechanical, acoustic, spectroscopic, thermodynamic and dynamical properties at finite temperature. The diagonalization of dynamic matrix is used to calculate the phonon dispersion curves (PDC) which provides the insight on the stability as it is the ironclad test which is used to check the dynamical stability. The calculated PDC for the haeck-BN along with the phonon density of states (PHDOS) are presented in Fig.4. The number of branches in the dispersion curve depends upon the number of atoms, if there are N atoms in the unit cell, there are 3N branches to the dispersion relation having 3 acoustical and 3N–3 optical modes.[53] There are eight atoms in the unit cell of haeck-BN for which there are 24 phonon branches whereas in 2D h-BN two atoms per unit cell results in to six phonon branches.[55,58,59] Each mode is labeled according to its polarization, the letter 'L', 'T' and 'Z' stands for longitudinal, transverse and out-of-plane vibrations,

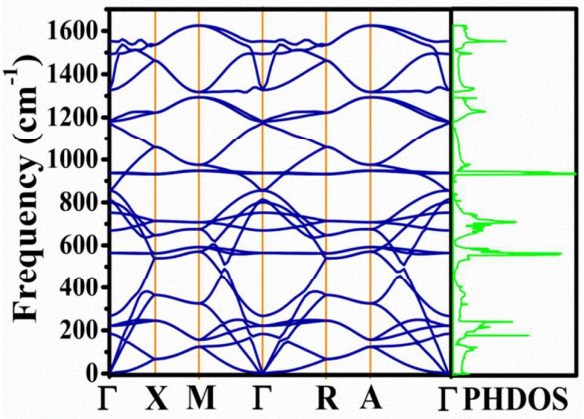

Fig. 4 Phonon dispersion curve along with the phonon density of states (PHDOS)

respectively. The letter 'A' and 'O' represent the acoustic and optical modes respectively. The longitudinal acoustic (LA) and transverse acoustic (TA) modes show linear dispersion around the Γ point, while the out of plane acoustic (ZA) mode exhibits quadratic dispersion, which is the characteristic feature of 2D layered materials.[21,59,60] This quadratic behavior of the ZA band which arises due to D6h point group symmetry, can be attributed to the fact that, at lowest order amplitude, strain energy which is induced by this vibration is altogether associated with the arching of this out-of-plane bending mode which is induced in the monolayer.[61]

The PDC plotted in high symmetry directions of the BZ does not have any phonon modes with imaginary frequency throughout BZ indicating dynamical stability of haeckelite BN like other haeckelite compounds.[32,33] The in-plane longitudinal and transverse modes have linear dispersion near the zone center (Γ- point), whereas the out-of-plane (ZA) mode has quadratic dispersion when **q** approaches to zero. The quadratic ZA mode is closely associated with the bending rigidity and lattice heat capacity of the nanosheet for the long-wavelength (small $\bar{q}$) region. On the other hand, a softening of the transverse acoustic (TA) and longitudinal acoustic (LA) modes is observed, indicating reduced group velocities. It is noteworthy that these reduced group velocities can be of use in improving the thermoelectric figure of merit ZT as it reduces the thermal conductivity. [62] The ZA mode which behaves greatly different from TA and LA modes will have further lower group velocity due to a parabolic dispersion near the **Γ**point. There is no gap observed in between acoustic and optical branches due to less mass difference between boron and nitrogen atoms similar to h-BN.[59] The phonons of the haeck-BN sheet shows a considerable softening compared to h-BN sheet which can be attributed to the fact that the elastic constants of haeck-BN may be smaller than the same of h-BN. In PDC of BN haeckelite at **Γ** point we observed nine singly (A) and six doubly (E) degenerated optical phonon modes i.e. **Γ= 9A+6E**. All 24 modes in BN- haeckelite are equally distributed in frequencies from 0 to ≈1600 cm^{-1}. The stability is further confirmed by calculating the PHDOS which is at the right panel of the Fig. 4. The phonon density of states is an important dynamical property, as its computation needs phonon frequencies in the entire Brillouin zone and can be defined as[63]

$$g(\omega) = \frac{1}{N}\int_{BZ}\sum_j \delta\left[\omega - \omega_j(\bar{q})\right]d\bar{q} \qquad (2)$$

where N being a normalization constant that $\int g(\omega)\, d\omega$ =1. $g(\omega)\, d\omega$ is the ratio of the number of eigenstates in the frequency interval $(\omega, \omega + d\omega)$ to the total number of eigenstates $\omega_j(\bar{q})$ is the phonon frequency of the j^{th} phonon modes. The PHDOS calculation is a real test which not only helps us to calculate lattice specific heat but also other thermodynamic function in the entire BZ.[64,65] The ionic bonding between the sp^2 hybridized B and N atoms in haeck-BN are predominant in the high-frequency modes, which is quite similar to the phonon modes in earlier reported sp^2 hybrid boron nitride structures.[59,66]

In the case of lower frequency region, the modes show dispersive behavior. This convergence can be attributed to close sharing of potential energy in the various modes. Since the dispersion of modes depends on the strength of interaction, a mixing character of modes due to repulsion gives

View Article Online
DOI: 10.1039/C8TB01649F

different variation. Whole phonon modes from **Γ-X** come close and keep same nature from **X-M** but split from **M-Γ** direction of BZ. The intense peaks at ≈ 600 and 900 cm^{-1} are attributed to the flat bands in dispersion curves. The additional weak singularity in the low frequency region is due to some of the strongly dispersed acoustical and low frequency optical phonon modes.

3.3 Adsorption Mechanisms

To understand the mechanism of the interaction between haeck-BN and nucleobases, we have first constructed a supercell (2x3) of haeck-BN with 48 atoms (24 B and 24 N atoms) to provide large surface for nucleobases to interact. The full structural optimization of haeck-BN sheet and all considered nucleobases adenine (A), thymine (T), guanine (G), cytosine (C) and uracil (U) is done individually. The optimized structure of nucleobases adenine, thymine, guanine, cytosine and uracil are presented in Fig. 5 (a-e).

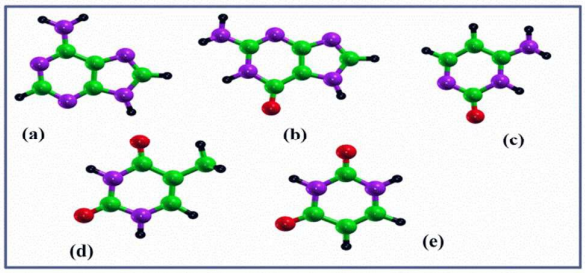

Fig. 5 Optimized structures of five nucleobases A, G, C, T and U. Red, green, black and purple ball corresponds to oxygen, carbon, hydrogen and nitrogen atoms respectively.

Fig. 6 (a-f) shows the optimized geometries of pristine haeck-BN sheet and nucleobase adsorbed haeck-BN sheet. We have chosen parallel orientation for all nucleobases over haeck-BN as previous works suggest the parallel position by the nucleobases over BN nanostructures due to its most stable configuration.[67,68] Our calculations of structural relaxation started by placing the molecule near the surface of haeckelite-BN initially which was followed by full structural relaxation to obtain the ground state geometrical configuration. In the energetically stable configuration of all the considered systems, the adsorbed molecules attained a distance in the range of 2.5-2.9 Å. This large distance of molecules from the haeckelite-BN monolayer prevents the formation of chemical bonds leading to the physisorption of the adsorbed molecules. Further, to confirm the absorption nature and distance of nucleobases from haeckelite-BN, we performed total energy calculation of each system with molecules at distances varying in the range 1-4 Å from the haeckelite-BN. We found that the minimum energy configuration is obtained all adsorbed molecules are placed at distance in the range of 2.5-2.9 Å from haeckelite-BN surface which supports our full structural relaxation calculation. We have also considered various orientations of nucleobases for better clarification we have tabulated the total energies of various configurations considered with different distance and orientation in Table S1 and S2 of Supplementary Information. The nature of the adsorption is physical (physisorption) as the distance between the nucleobases and haeck-BN sheet is large like ~ 2.8 Å (as can be seen in Table 1). The large distance between nucleobases and haeck-BN sheet ensures the elimination of the possibility of any covalent bond formation. The long range van der Waals interactions were taken into account with the incorporation of dispersion corrected DFT (DFT-D2) in the present calculations as it increases binding/adsorption about 8 to10 times than the normal PBE calculation.[69] We have not used new D3[70] correction as both D2 and D3 gives similar results in case of non-covalent interaction.[71] The Adsorption energy, E_{ad} calculated for A, G, C, T and U over haeck-BN are -0.662 eV, -0.742 eV, -0.660 eV, -0.668 eV and -0.525 eV respectively with binding distance **d** between 2.7 Å to 2.9 Å. Our adsorption energy results are better than the previously reported values of adsorption energy for h-BN as well as graphene [42,72–74] which can be attributed to the special and different structural and electronic properties of haeck-BN.

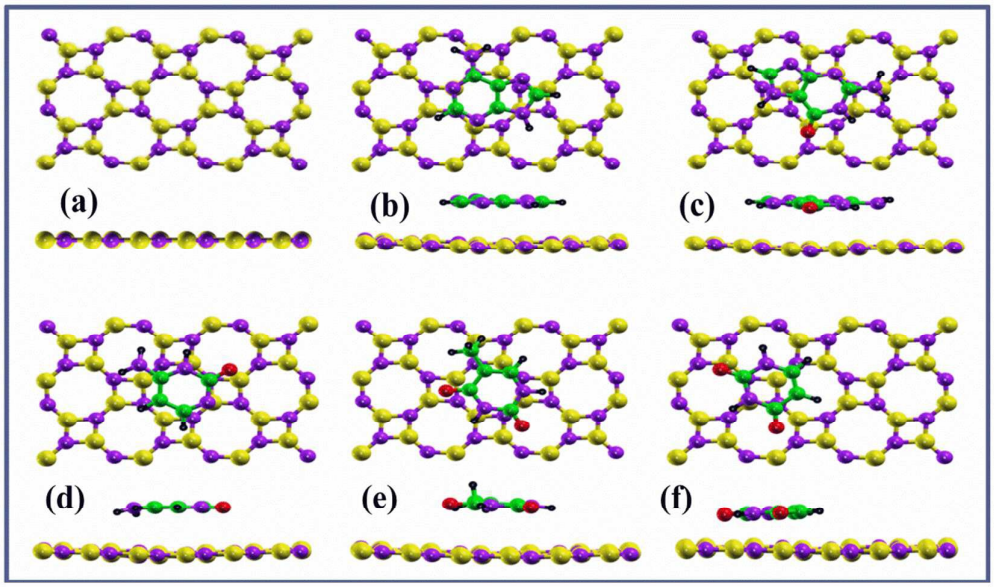

Fig. 6 Optimized structures of (a) pristine haeck-BN and nucleobases adsorbed haeck-BN (b) Adenine (c) Guanine (d) Cytosine (e) Thymine (f) Uracil (top and side view).

View Article Online
DOI: 10.1039/C8TB01649F

However, the sequence of the adsorption of the nucleobases molecule over haeck-BN (G > T > A ≈ C > U) is similar to the adsorption trend of nucleobases with other BN and carbon nanostructures.[42,72–74] A comparative results regarding adsorption energy of all five nucleobases on different nanomaterial are shown in Fig. 7. The van der Waals forces together with the stacking of the molecules with the surface is the reason behind this difference in the adsorption energy.[75,76] The π – π stacking configuration has higher adsorption energy as it minimizes the repulsion due to π orbital overlapping to prevent the molecules to get repel from the nanosurface. This leads to the superior adsorption energy on nanosurface.[44,45]

The present results depict that the nucleobases are more effectively adsorbed on hacek-BN compared to graphene,[73,74] and other boron nitride nanostructures such as h-BN,[42] BNNR[68] and BNNT.[77] The adsorption of molecules over haeck-BN sheet alter the electronic properties which have been inspected by calculating the band dispersion, band gap, density of states (DOS) and partial DOS (PDOS). The band dispersion curve of pristine and nucleobases adsorbed haeck-BN sheet are presented in Fig. 8. A significant change in the band structure as well as band gap can be seen from the band dispersion. There are some impurity states generated within the band structure of pristine haeck-BN after the adsorption of nucleobases which is mainly due to the p orbital electron of C, O and N atoms and a partial contribution of s orbital of H atom present in the nucleobase molecule. Appearance of peculiar flat bands in the conduction as well as valence band region in the band structure is also observed after the adsorption of nucleobase. This is an interesting feature which can be attributed to the quenching of the kinetic energy of the electrons [78]. The band structure after the adsorption of adenine on the surface of haeck-BN is depicted in Fig. 8 (b) which shows the appearance of impurity states as flat bands at the top of the valence band region after adenine adsorption. These flat bands are created due to participation of p_x orbital electron of nitrogen and carbon atoms present in the adenine molecule. In the valence band region near -1.9 eV and -4 eV (due to p_x orbital of N) and in the conduction band region near 2 eV (due to p_x orbital of C) flat bands are observed. A similar behavior of bands in the band dispersion is observed for all nucleobases. In all nucleobases other than adenine, oxygen

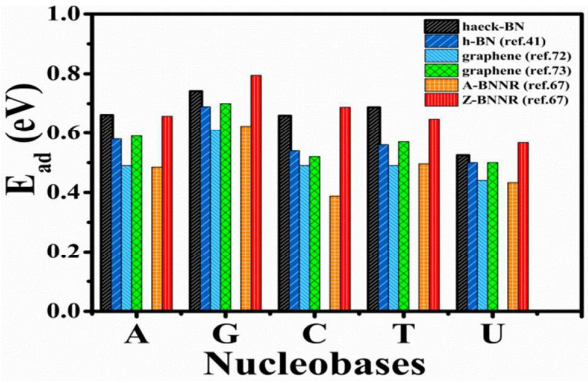

Fig. 7 Comparative adsorption energies plot of nucleobases with different nanostructures

atom also takes part in the formation of flat bands. In guanine (Fig. 8 (c)) oxygen p_x orbital plays role in the valence band region near -3 eV. However, after the adsorption of cytosine on the haeck-BN surface a large modulation in the band gap is observed (Fig. 8 (d)). Many flat bands in band structure are generated in valence as well as conduction bands. This is a similar modification in the bands after thymine, however uracil creates less number of flat bands that too only in the

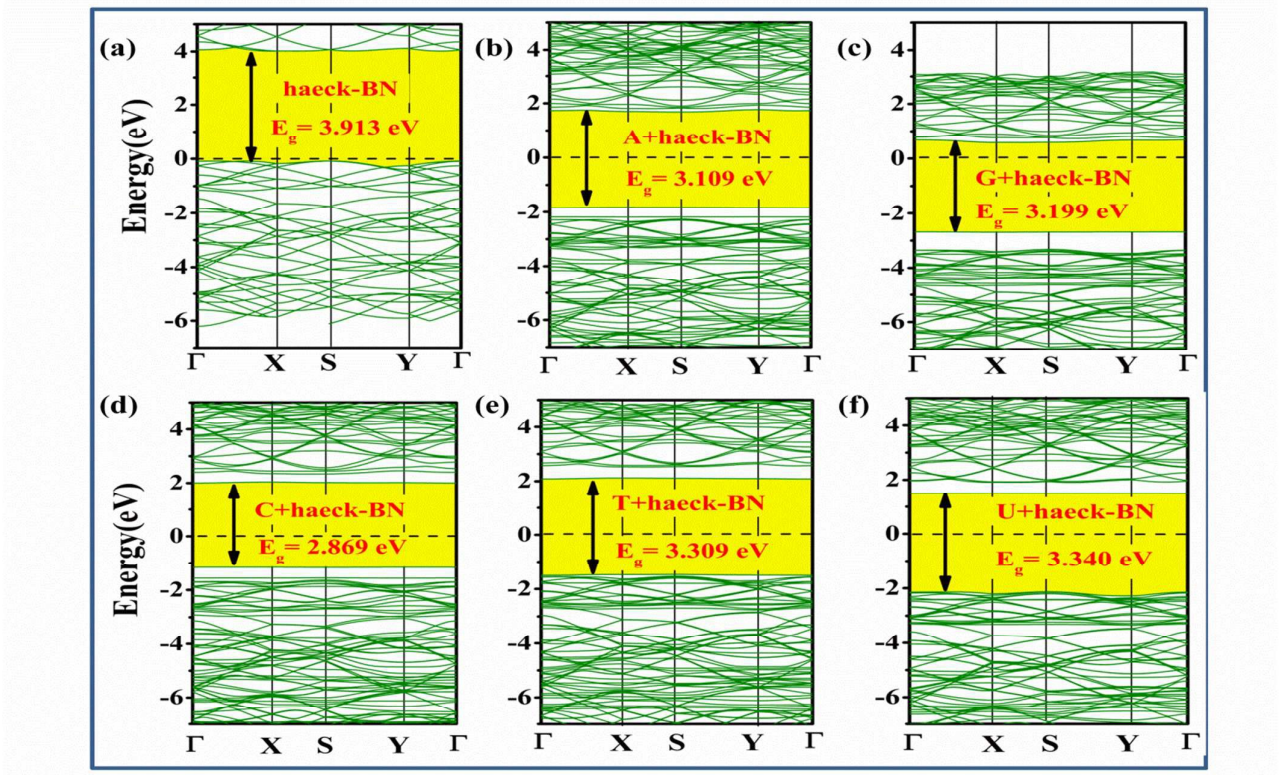

Fig. 8 Band structure plots of haeck-BN (a) pristine and nucleobase adsorbed (b) Adenine (c) Guanine (d) Cytosine (e) Thymine (f) Uracil.

View Article Online
DOI: 10.1039/C8TB01649F

conduction band which can be attributed to its size and number of atoms available to participate in the formation extra electronic states (Fig. 8 (e-f)). The band gap of haeck-BN reduces from 3.913 eV to 3.199 eV, 2.999 eV, 2.869 eV, 3.309 eV and 3.340 eV respectively after adsorption of nucleobases A, G, C, T and U. We further analyzed the electron transport by calculating the Lowdin charge transfer. The significant charge transfer between the nucleobase and haeck BN in the adsorption process shows that the interaction of nucleobase can lead to modifications of structure and electronic properties of haeck-BN. A significant charge transfer of 0.14e, 0.15e, 0.10e, 0.11e and 0.09e for A, G, C, T and U respectively may be the reason for the bandgap modulation. The charge transfer can also be understood by charge density and HOMO-LUMO calculations.

The effect of these molecule on the charge density of the pristine haeck-BN are understand by charge density calculations as it helps to predict the chemical bonding and also the charge transfer behavior between haeck-BN and nucleobases. The calculated charge density contours are presented in Fig S3 of the supplementary material.

The Highest Occupied Molecular Orbital which is abbreviated as HOMO and the Lowest Unoccupied Molecular Orbital as LUMO are the representatives of any systems ability to donate or accept electron. In the collective form they both are known as Frontier Molecular Orbital. These orbitals are considered as the main orbitals which involves in the chemical stability which are situated to the adjacent side of Fermi level which also bring light to understand the electronic state present near Fermi level and also the transfer of electrons. The systematic representation of HOMO and LUMO orbitals for all considered systems are shown in Fig. S4 of the electronic supplementary material. From the figure we can see that the electronic cloud in both orbitals in the pristine Haeckelite-BN was distribution over whole structure. Electron cloud in HOMO is mainly due to the N atom while LUMO is due to B atom throughout the structure this means that the electron states near the Fermi is due to p orbital of B and N atoms. These orbital can capture or lose electrons. We see large difference in the HOMO and LUMO orbital electron clouds of the pristine haeckelite-BN after the adsorption of nucleobases (Fig.S4). In all nucleobases adsorbed haeck-BN system the LUMO are more localized on N and O atoms which clearly meant that the electron transfer is mainly done between the N and O atoms of nucleobases and the HOMO orbital of haeck-BN which is localized over B atoms.

To understand the molecular contribution in the electronic properties, we have calculated the density of states (DOS) and partial density of state (PDOS) of pristine and nucleobases adsorbed haeck-BN which are presented in Fig. 9 and Fig s1 (in the supplementary material). The major advantage of DOS as well as PDOS calculation is that one can easily analyze the contribution of electronic states by the adsorbed molecule. The Fig. 9 clearly shows that the valance band of pristine haeck-BN has the major contribution to the Fermi level. The interaction of haeck-BN with the nucleobases results in small peaks in the valence band region near Fermi level at -1.5 eV, -1.9 eV and -2.5 eV in case of C, A and G respectively. However, among these three, only C contributes in the conduction band. Some states are generated at 1.7 eV and 2 eV in the conduction band region in case of U and T respectively. From the DOS it is clear that all nucleobases alters the electronic properties of haeck-BN significantly with major contribution in the lower valence band region between -10 eV to -15 eV where the impurity states have been generated from the interaction of molecules and haeck-BN. Major contribution arises from the p orbit electrons which create the extra peak. Cytosine modulates the band gap of pristine haeck-BN by large amount (1.04 eV) due to the appearance of some extra electronic states from the presence of NH_2 group in the molecule. Among all five nucleobases, guanine has large adsorption energy over haeck-BN due to its specific structural and electronic properties. The presence of oxygen atom which is a strong electron donor in guanine makes it to get strongly bound to haeck-BN surface. The extra pentagon with C, N and O atoms induces the molecule to exhibit more polarization. The higher electronegativity of N and O atoms induces greater binding.[72,79]

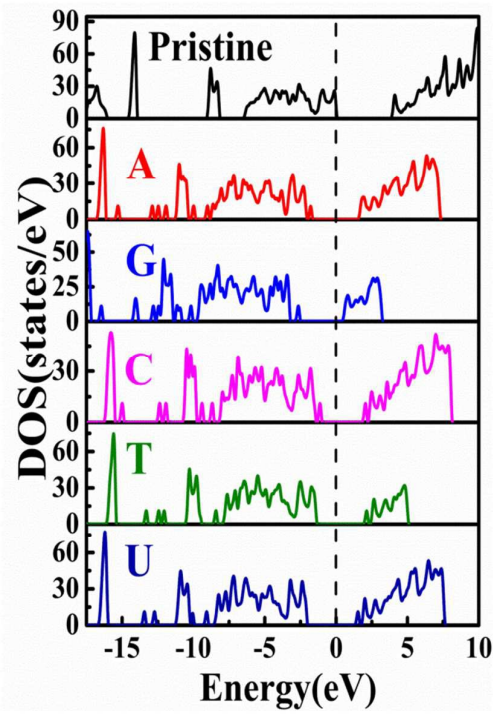

Fig. 9 Electronic density of states (DOS) plot of pristine haeck-BN along with nucleobase adsorbed nucleobases.

The value of energy gap, E_g is an important factor to ascertain the electrical conductivity (σ) of materials because the energy required for emancipate an electron from the outer shell to become a free portable charge carrier is equivalent to bandgap.

The classic relation between the E_g and electrical conductivity of a material can be expressed by the following relation:[80]

$$\sigma \propto e^{-E_g/2KT} \quad (3)$$

where k and T are the Boltzmann's constant and the temperature respectively. According to eqn. (3), the relation between the conductivity is inversely proportional to the bandgap means smaller the value of bandgap E_g, higher is the electrical conductivity at given temperature T. Thus, after the adsorption of nucleobases over haeck-BN surface significant decrement in the band gap indicates an increase in the σ of

View Article Online
DOI: 10.1039/C8TB01649F

the haeck-BN sheet. The σ increases in the order of C > G > A > T > U adsorbed haeck-BN respectively. Therefore, after adsorption of nucleobase, the energy gap changes and becomes narrower; consequently, increases the conductivity of the nanosheet confirming the strong interaction between the molecule and the haeck-BN. The change in the Fermi level of haeck-BN due to the nucleobases causes an electrical signal, and therefore it could be potentially used in biosensor applications.

Table 2 Adsorption energy Ead(eV), vertical distance d (Å) of nucleobases from haeck-

System	haeck-BN	A	G	C	T	U
E_g(eV)	3.913	3.109	3.199	2.869	3.309	3.340
Δ E_g (eV)	-	0.714	0.914	1.044	0.604	0.573
E_{ad} (eV)	-	-0.662	-0.742	-0.660	-0.668	-0.525
d (Å)	-	2.945	2.745	2.775	2.725	2.953
E_F	-4.199	-1.617	-0.424	-2.322	-2.344	-1.798
Φ (eV)	5.972	3.896	2.837	4.455	4.503	3.914

BN, bandgap Eg (eV) and Fermi energy EF (eV).

In order to check the novelty of haeck-BN as a carrier of nucleobases and its reusability, we have calculated the recovery time. The recovery time is the renowned parameter to decide the superiority of any sensor or detector or carrier with respect to the other. Generally experimentalist find the recovery time by heating the substrate. However, the theoretical approach to estimate the recovery time is based on transition theory. The required equation can be expressed as,[81]

$$\tau = \upsilon^{-1} e^{-E_{ads}/KT} \quad (4)$$

Where υ is the attempt frequency, K is the Boltzmann constant (~8.318 $*10^{-3}$ kJ/mol K) and T is the temperature. We use the value of attempt frequency as 10^{12} s^{-1} [81–83] and temperature 298K, which has been employed to measure the recovery time for CNT from NO_2 molecule. Ultra-fast recovery time of 292 ms (millisecond), 130 ms, 120 ms, 160 ms and 0.6 ms is predicted for haeck-BN by using this attempt frequency for G, A, C, T and U respectively.

We have also calculated the work function of pristine as well as nucleobase adsorbed haeck-BN sheet to further check the sensing capability of nucleobases. The work function **ϕ**(eV) is the amount of energy required to remove an electron from the highest filled level in the Fermi distribution of any material to a point in a field-free zone just outside the solid at absolute zero temperature.[53]

$$\phi(eV) = E_{vac} - E_F \quad (5)$$

where E_{vac} is the energy at vacuum level and E_F is Fermi level energy. By integrating the density of states from the lowest energy level to an energy level that gives the total number of electrons in the unit cell is determined as the Fermi energy level E_F, and the E_{vac} is obtained by the planar-average electrostatic potential energy along the z direction which is the direction of vacuum.[53] The **ϕ** plots are shown in Fig. S2 of supplementary material. There are two negative peaks on the curves of electrostatic potentials, and the strong and weak peaks corresponds the positions of the haeck-BN nanosheet and the nucleobases respectively. The difference of the electrostatic potential between Fermi and vacuum levels is the work function. The **ϕ** for haeck-BN shows a significant decrement after the adsorption of nucleobases. The **ϕ** of pristine haeck-BN is calculated as 5.972 eV which is comparatively higher than other BN nanostructures.[68,84] Large decrement in the **ϕ** of haeck-BN is observed after the adsorption of nucleobase on its surface. The modulation of **ϕ** has following trend: G (3.135eV) > A (2.076eV) ≈ U (2.058) > C (1.517eV) ≈ T (1.469eV). The calculated work functions are shown in Table 2. The change in work function explains the physical adsorption of nucleobases on the surface of haeck-BN results due to strong nucleobases-haeck-BN interaction. The large decrement in the work function enhances the photocatalysis as we know lower the work function greater the catalytic activity. The modulation of electronic properties after adsorption of nucleobases on haeck-BN is clearly evident in our results which further suggest an easy detection of nucleobases by haeck-BN.

Finally from the all above results we can say that the nucleobases molecules gets physically adsorbed on the haeck-BN surface which is good to utilize this new boron nitride cousin for targeted delivery of these biomolecule as reversibility is easy in case of physisorption than from chemisorption. Results which we found indicate that the haeck-BN is a good candidate for biomolecule carrier and should be explored more for its biomedical applications and also in photocatalysis.

4. Conclusions

Using the state-of-the-art first principles calculations based on density functional theory, we investigated the electronic properties of relatively newly proposed Haeckelite BN comprising of square and octagonal rings. The kinetic stability of this haeckelite monolayer has been confirmed by phonon dispersion curves and the phonon density of states. There is not a single mode with imaginary frequency in the entire BZ. The calculated electronic properties of this new BN haeckelite form illustrate its direct bang gap semiconducting behavior which is the main advantage of any material to utilize in chemical as well as bio sensor. To understand the adsorption behavior of the nucleobases on haeck-BN surface, we have employed van der Waals corrections (DFT-D2) to the density functional theory. The comparative analysis of the adoption mechanism of nucleobases with graphene, BNNT and haeck-BN is discussed in detail and showed superiority. Our result depicts the physisorption of nucleobases on the surface of haeck-BN with the interactions order of G > T > A ≈ C > U respectively. The change in work function after the adsorption of nucleobases was also calculated and changes were found in order G (3.135eV) > A (2.076eV) ≈ U (2.058) > C (1.517eV) ≈ T (1.469eV) respectively which is different from both graphene

View Article Online
DOI: 10.1039/C8TB01649F

and BNNT, and it confirms sensitivity towards the nucleobases. For the further confirm the novelty of the haeck-BN as bio sensor we have calculated the recovery time. Very less recovery time of 292 ms, 130ms, 120ms, 160ms and 0.6ms is predicted for G, A, C, T and U respectively which reinforced the possibility of haeck-BN for reusable biosensor. The large change in the electronic properties gives the idea of the interaction and its possible use for the detection of these bio molecules. Thus from our results, one may conclude that the haeck-BN may act as an alternative candidate for the sensing application of nucleobases as well as DNA sequencing other than h-BN and graphene systems. We hope that our results will motivate more experimental and theoretical studies on new layered III-V semiconducting materials.

Conflicts of interest

There are no conflicts to declare.

Acknowledgements

The study is financially supported by a research project from Science and Engineering Research Board (SERB) (SB/S2/CMP-0005/2013), Govt. of India. The computations are carried out using high performance computer cluster provided under DST-FIST program.

Notes and references

1 W. Krätschmer, L. D. Lamb, K. Fostiropoulos and D. R. Huffman, Solid C60: a new form of carbon, *Nature*, 1990, **347**, 354–358.
2 D. S. Bethune, C. H. Kiang, M. S. de Vries, G. Gorman, R. Savoy, J. Vazquez and R. Beyers, Cobalt-catalysed growth of carbon nanotubes with single-atomic-layer walls, *Nature*, 1993, **363**, 605–607.
3 L. S. Ying, M. A. Bin Mohd Salleh, H. B. Mohamed Yusoff, S. B. Abdul Rashid and J. B. Abd. Razak, Continuous production of carbon nanotubes - A review, *J. Ind. Eng. Chem.*, 2011, **17**, 367–376.
4 K. S. Novoselov, A. K. Geim, S. V. Morozov, D. Jiang, Y. Zhang, S. V. Dubonos, I. V. Grigorieva and A. A. Firsov, Electric Field Effect in Atomically Thin Carbon Films, *Science*, 2004, **306**, 666–669.
5 E. Pop, V. Varshney and A. K. Roy, Thermal properties of graphene: Fundamentals and applications, *MRS Bull.*, 2012, **37**, 1273–1281.
6 X. Wang, L. Zhi and K. Müllen, Transparent, conductive graphene electrodes for dye-sensitized solar cells, *Nano Lett.*, 2008, **8**, 323–327.
7 J. H. Chen, M. Ishigami, C. Jang, D. R. Hines, M. S. Fuhrer and E. D. Williams, Printed graphene circuits, *Adv. Mater.*, 2007, **19**, 3623–3627.
8 Y. Zhang, Y. W. Tan, H. L. Stormer and P. Kim, Experimental observation of the quantum Hall effect and Berry's phase in graphene, *Nature*, 2005, **438**, 201–204.
9 S. V. Morozov, K. S. Novoselov, M. I. Katsnelson, F. Schedin, D. C. Elias, J. A. Jaszczak and A. K. Geim, Giant intrinsic carrier mobilities in graphene and its bilayer, *Phys. Rev. Lett.*, 2008, **100**, 016602–016606.
10 J. H. Chen, C. Jang, S. Adam, M. S. Fuhrer, E. D. Williams and M. Ishigami, Charged-impurity scattering in graphene, *Nat. Phys.*, 2008, **4**, 377–381.
11 S. S. Gregersen, S. R. Power and A. P. Jauho, Nanostructured graphene for spintronics, *Phys. Rev. B*, 2017, **95**, 121406–121411.
12 F. Molitor, J. Güttinger, C. Stampfer, S. Dröscher, A. Jacobsen, T. Ihn and K. Ensslin, Electronic properties of graphene nanostructures, *J. Phys. Condens. Matter*, 2011, **23**, 243201-243215.
13 J. Klinovaja and D. Loss, Spintronics in MoS2 monolayer quantum wires, *Phys. Rev. B.*, 2013, **88**, 075404–075410.
14 Y. Xu, Z. Gan and S. C. Zhang, Enhanced thermoelectric performance and anomalous seebeck effects in topological insulators, *Phys. Rev. Lett.*, 2014, **112**, 226801–226805.
15 Y. N. Xu and W. Y. Ching, Calculation of ground-state and optical properties of boron nitrides in the hexagonal, cubic, and wurtzite structures, *Phys. Rev. B*, 1991, **44**, 7787–7798.
16 W. Choi, N. Choudhary, G. H. Han, J. Park, D. Akinwande and Y. H. Lee, Recent development of two-dimensional transition metal dichalcogenides and their applications, *Mater. Today*, 2017, **20**, 116–130.
17 K. Takeda and K. Shiraishi, Theoretical possibility of stage corrugation in Si and Ge analogs of graphite, *Phys. Rev. B*, 1994, **50**, 14916–14925.
18 S. Cahangirov, M. Topsakal, E. Aktürk, H. Šahin and S. Ciraci, Two- and one-dimensional honeycomb structures of silicon and germanium, *Phys. Rev. Lett.*, 2009, **102**, 236804–236808.
19 H. Liu, A. T. Neal, Z. Zhu, Z. Luo, X. Xu, D. Tománek and P. D. Ye, Phosphorene: An unexplored 2D semiconductor with a high hole mobility, *ACS Nano*, 2014, **8**, 4033–4041.
20 S. B. Pillai, S. Narayan, S. D. Dabhi and P. K. Jha, First principles calculation of two dimensional antimony and antimony arsenide, *AIP Conf. Proc.*, 2016, **1731**, 090024–090027.
21 S. B. Pillai, S. D. Dabhi, S. Narayan and P. K. Jha, Strain Effect on Electronic and Lattice Dynamical Behaviour of Two Dimensional Bi , BiAs and BiSb, *AIP Conf. Proc.*, 2018, **1942**, 090022–090025.
22 B. Feng, J. Zhang, Q. Zhong, W. Li, S. Li, H. Li, P. Cheng, S. Meng, L. Chen and K. Wu, Experimental realization of two-dimensional boron sheets, *Nat. Chem.*, 2016, **8**, 563–568.
23 A. Pakdel, C. Zhi, Y. Bando and D. Golberg, Low-dimensional boron nitride nanomaterials, *Mater. Today*, 2012, **15**, 256–265.
24 J. Yin, L. Jidong, Y. Hang, Y. Jin, G. Tai, L. Xuemei, Z. Zhang and W. Guo, Boron Nitride Nanostructures: Fabrication, Functionalization and Applications, *Small*, 2016, **12**, 2942–2968.
25 A. Pakdel, Y. Bando and D. Golberg, Nano boron nitride flatland, *Chem. Soc. Rev.*, 2014, **43**, 934–959.
26 C. R. Dean, A. F. Young, I. Meric, C. Lee, L. Wang, S. Sorgenfrei, K. Watanabe, T. Taniguchi, P. Kim, K. L. Shepard and J. Hone, Boron nitride substrates for high-quality graphene electronics, *Nat. Nanotechnol.*, 2010, **5**, 722–726.
27 P. Sutter, J. Lahiri, P. Zahl, B. Wang and E. Sutter, Scalable synthesis of uniform few-layer hexagonal boron nitride dielectric films, *Nano Lett.*, 2013, **13**, 276–281.
28 X. Li, J. Yin, J. Zhou and W. Guo, Large area hexagonal boron nitride monolayer as efficient atomically thick insulating coating against friction and oxidation, *Nanotechnology*, 2014, **25**, 105701–105705.
29 G. H. Lee, Y. J. Yu, C. Lee, C. Dean, K. L. Shepard, P. Kim and J. Hone, Electron tunneling through atomically flat and ultrathin hexagonal boron nitride, *Appl. Phys. Lett.*, 2011, **99**, 243114–243116.
30 Q. Li, X. Zou, M. Liu, J. Sun, Y. Gao, Y. Qi, X. Zhou, B. I. Yakobson, Y. Zhang and Z. Liu, Grain Boundary Structures

View Article Online
DOI: 10.1039/C8TB01649F

and Electronic Properties of Hexagonal Boron Nitride on Cu(111), *Nano Lett.*, 2015, **15**, 5804–5810.
31 Y. Liu, X. Zou and B. I. Yakobson, Dislocations and Grain Boundaries in Two-Dimensional Boron Nitride, *ACS Nano*, 2012, **6**, 7053–7058.
32 D. C. Camacho-Mojica and F. López-Urías, GaN Haeckelite Single-Layered Nanostructures: Monolayer and Nanotubes, *Sci. Rep.*, 2015, **5**, 1–11.
33 P. V. Gaikwad, P. K. Pujari, S. Chakroborty and A. Kshirsagar, Cluster assembly route to a novel octagonal two-dimensional ZnO monolayer, *J. Phys. Condens. Matter*, 2017, **29**, 335501–335516.
34 X. Tu, S. Manohar, A. Jagota and M. Zheng, DNA sequence motifs for structure-specific recognition and separation of carbon nanotubes, *Nature*, 2009, **460**, 250–253.
35 D. Umadevi and G. N. Sastry, Quantum mechanical study of physisorption of nucleobases on carbon materials: Graphene versus carbon nanotubes, *J. Phys. Chem. Lett.*, 2011, **2**, 1572–1576.
36 C. Zhi, Y. Bando, W. Wang, C. Tang, H. Kuwahara and D. Golberg, DNA-mediated assembly of boron nitride nanotubes, *Chem. Asian J.*, 2007, **2**, 1581–1585.
37 G. Ciofani, V. Raffa, A. Menciassi and A. Cuschieri, Cytocompatibility, interactions, and uptake of polyethyleneimine-coated boron nitride nanotubes by living cells: Confirmation of their potential for biomedical applications, *Biotechnol. Bioeng.*, 2008, **101**, 850–858.
38 X. Chen, P. Wu, M. Rousseas, D. Okawa, Z. Gartner, A. Zettl and C. R. Bertozzi, Boron Nitride Nanotubes Are Noncytotoxic and Can Be Functionalized for Interaction with Proteins and Cells, *J. AM. CHEM. SOC.*, 2009, **131**, 890–891.
39 S. Liu, B. Lu, Q. Zhao, J. Li, T. Gao, Y. Chen, Y. Zhang, Z. Liu, Z. Fan, F. Yang, L. You and D. Yu, Boron nitride nanopores: Highly sensitive DNA single-molecule detectors, *Adv. Mater.*, 2013, **25**, 4549–4554.
40 L. Zhang and X. Wang, DNA Sequencing by Hexagonal Boron Nitride Nanopore: A Computational Study, *Nanomaterials*, 2016, **6**, 111-121.
41 Y. Zhao, Y. Xie, Z. Liu, X. Wang, Y. Chai and F. Yan, Two-dimensional material membranes: An emerging platform for controllable mass transport applications, *Small*, 2014, **10**, 4521–4542.
42 Q. Lin, X. Zou, G. Zhou, R. Liu, J. Wu, J. Li and W. Duan, Adsorption of DNA/RNA nucleobases on hexagonal boron nitride sheet: an ab initio study, *Phys. Chem. Chem. Phys.*, 2011, **13**, 12225-12230.
43 K. Jin, L. Xie, Y. Tian and D. Liu, Au-Modified Monolayer MoS_2 Sensor for DNA Detection, *J. Phys. Chem. C*, 2016, **120**, 11204–11209.
44 G. Ciofani, V. Raffa, J. Yu, Y. Chen, Y. Obata, S. Takeoka, A. Menciassi and A. Cuschieri, Boron Nitride Nanotubes: A Novel Vector for Targeted Magnetic Drug Delivery, *Curr. Nanosci.*, 2009, **5**, 33–38.
45 G. G. Genchi and G. Ciofani, Bioapplications of boron nitride nanotubes, *Nanomedicine*, 2015, **10**, 3315–3319.
46 Z. Zhang, H. Huang, X. Yang and L. Zang, Tailoring electronic properties of graphene by π- π Stacking with aromatic molecules, *J. Phys. Chem. Lett.*, 2011, **2**, 2897–2905.
47 T. Kar, H. F. Bettinger, S. Scheiner and a K. Roy, Noncovalent π- π Stacking and CH---π Interactions of Aromatics on the Surface of Single-Wall Carbon Nanotubes: An MP2 Study, *J. Phys. Chem. C*, 2008, **112**, 20070–20075.
48 P. Giannozzi, S. Baroni, N. Bonini, M. Calandra, R. Car, C. Cavazzoni, D. Ceresoli, G. L. Chiarotti, M. Cococcioni, I. Dabo, A. Dal Corso, S. De Gironcoli, S. Fabris, G. Fratesi, R. Gebauer, U. Gerstmann, C. Gougoussis, A. Kokalj, M. Lazzeri, L. Martin-Samos, N. Marzari, F. Mauri, R. Mazzarello, S. Paolini, A. Pasquarello, L. Paulatto, C. Sbraccia, S. Scandolo, G. Sclauzero, A. P. Seitsonen, A. Smogunov, P. Umari and R. M. Wentzcovitch, QUANTUM ESPRESSO: A modular and open-source software project for quantum simulations of materials, *J. Phys. Condens. Matter*, 2009, **21**, 395502–395521.
49 J. D. Head and M. C. Zerner, A Broyden-Fletcher-Goldfarb-Shanno optimization procedure for molecular geometries, *Chem. Phys. Lett.*, 1985, **122**, 264–270.
50 J. P. Perdew, K. Burke and M. Ernzerhof, Generalized Gradient Approximation Made Simple, *Phys. Rev. Lett.*, 1996, **77**, 3865–3868.
51 H. J. Monkhorst and J. D. Pack, Special points for Brillouin-zone integrations, *Phys. Rev. B.*, 1976, **13**, 5188–5192.
52 S. Baroni, S. De Gironcoli, A. Dal Corso and P. Giannozzi, Phonons and related crystal properties from density-functional perturbation theory, *Rev. Mod. Phys.*, 2001, **73**, 515–562.
53 C. Kittel, *Introduction to Solid State Physics*, John Wiley & Sons, Inc, United States, 2010.
54 S. Grimme, Semiempirical GGA-Type Density Functional Constructed with a Long-Range Dispersion Correction, *J. Comput. Chem.*, 2006, **27**, 1787–1799.
55 M. Topsakal, E. Aktürk and S. Ciraci, First-principles study of two- and one-dimensional honeycomb structures of boron nitride, *Phys. Rev. B.*, 2009, **79**, 115442–115452.
56 E. Kroumova, M. L. Aroyo, J. M. Perez-Mato, A. Kirov, C. Capillas, S. Ivantchev and H. Wondratschek, Bilbao Crystallographic Server: Useful databases and tools for phase-transition studies, *Phase Transitions*, 2003, **76**, 155–170.
57 S. Barua, H. S. Dutta, S. Gogoi, R. Devi and R. Khan, Nanostructured MoS2 Based Advanced Biosensors: A Review, *ACS Appl. Nano Mater.*, 2018, **1**, 2-25.
58 P. Anees, M. C. Valsakumar and B. K. Panigrahi, Effect of strong phonon–phonon coupling on the temperature dependent structural stability and frequency shift of 2D hexagonal boron nitride, *Phys. Chem. Chem. Phys.*, 2016, **18**, 2672–2681.
59 P. K. Jha and H. R. Soni, Strain induced modification in phonon dispersion curves of monolayer boron pnictides, *J. Appl. Phys.*, 2014, **115**, 023509-023517.
60 I. Lifshitz, Thermal properties of chain and layered structures at low temperatures, *Zh. Eksp. Teor. Fiz*, 1952, **22**, 475–486.
61 M. S. Dresselhaus, *Physical Properties of Carbon Nanotubes*, Imperial College Press, London, 2005.
62 C. Marchbanks and Z. Wu, Reduction of heat capacity and phonon group velocity in silicon nanowires, *J. Appl. Phys.*, 2015, **117**, 084305–084309.
63 J.-Y. Lin, P. L. Ho, H. L. Huang, P. H. Lin, Y.-L. Zhang, R.-C. Yu, C.-Q. Jin and H. D. Yang, BCS-like superconductivity in MgCNi3, *Phys. Rev. B*, 2003, **67**, 052501-052504.
64 P. K. Jha and S. P. Sanyal, A lattice dynamical study of the role of pressure on Raman modes in high-Tc HgBa2CuO4, *Physica C* , 1996, **261**, 259–262.
65 P. K. Jha, Phonon spectra and vibrational mode instability of MgCNi3, *Phys. Rev. B.*, 2005, **72**, 214502–214507.
66 W. Lu, X. Liu, S. Liu, W. Cao, Y. Zhang and P. Yang, Locus-specific Retention Predictor (LsRP): A Peptide Retention Time Predictor Developed for Precision Proteomics, *Sci. Rep.*, 2017, **7**, 1–9.
67 E. C. Anota, Y. Tlapale, M. S. Villanueva and J. A. R. Márquez, Non-covalent functionalization of hexagonal boron nitride nanosheets with guanine, *J Mol Model*, 2015, **21**, 215–221.
68 S. D. Dabhi, B. Roondhe and P. K. Jha, Nucleobases-decorated boron nitride nanoribbons for electrochemical biosensing: A dispersion-corrected DFT study, *Phys. Chem. Chem. Phys.*, 2018, **20**, 8943-8950.

View Article Online
DOI: 10.1039/C8TB01649F

69 B. Roondhe, S. D. Dabhi and P. K. Jha, Sensing properties of pristine boron nitride nanostructures towards alkaloids: A first principles dispersion corrected study, *Appl. Surf. Sci.*, 2018, **441**, 588-598.
70 S. Grimme, J. Antony, S. Ehrlich and H. Krieg, A consistent and accurate ab initio parametrization of density functional dispersion correction (DFT-D) for the 94 elements H-Pu, *J. Chem. Phys.*, 2010, **132**, 154104-154122.
71 J. B. A. Davis, F. Baletto and R. L. Johnston, The Effect of Dispersion Correction on the Adsorption of CO on Metallic Nanoparticles, *J. Phys. Chem. A*, 2015, **119**, 9703–9709.
72 N. Ding, X. Chen, C.-M. L. Wu and H. Li, Adsorption of nucleobase pairs on hexagonal boron nitride sheet: hydrogen bonding versus stacking, *Phys. Chem. Chem. Phys.*, 2013, **15**, 10767-10776.
73 S. Gowtham, R. H. Scheicher, R. Ahuja, R. Pandey and S. P. Karna, Physisorption of nucleobases on graphene: Density-functional calculations, *Phys. Rev. B.*, 2007, **76**, 033401–033404.
74 H. H. Gürel and B. Salmankurt, Binding mechanisms of DNA/RNA nucleobases adsorbed on graphene under charging: First-principles van der Waals study, *Mater. Res. Express*, 2017, **4**, 065401-065408.
75 P. Han, K. Akagi, F. Federici Canova, H. Mutoh, S. Shiraki, K. Iwaya, P. S. Weiss, N. Asao and T. Hitosugi, Bottom-up graphene-nanoribbon fabrication reveals chiral edges and enantioselectivity, *ACS Nano*, 2014, **8**, 9181–9187.
76 K. Müller-Dethlefs and P. Hobza, Noncovalent Interactions: A Challenge for Experiment and Theory, *Chem. Rev.*, 2000, **100**, 143–168.
77 S. Mukhopadhyay, S. Gowtham and R. H. Scheicher, Theoretical study of physisorption of nucleobases on boron nitride nanotubes : a new class of hybrid nano-biomaterials, *Nanotechnology*, 2010, **21**, 165703-165708.
78 Z. Gulácsi, Interaction-created effective flat bands in conducting polymers, *Eur. Phys. J. B*, 2014, **87**, 143–153.
79 F. Erkoç and Sakir Erkoç, Structural and electronic properties of guanine and guanosine, *J. Mol. Struct. THEOCHEM*, 2002, **589**, 405–411.
80 S. S. Li, *Semiconductor Physical Electronics*, Springer Science, United States, 1997.
81 Z. Rostami, M. Pashangpour and R. Moradi, DFT study on the chemical sensing properties of B24N24nanocage toward formaldehyde, *J. Mol. Graph. Model.*, 2017, **72**, 129–135.
82 S. Peng, K. Cho, P. Qi and H. Dai, Ab initio study of CNT NO2gas sensor, *Chem. Phys. Lett.*, 2004, **387**, 271–276.
83 K. Patel, B. Roondhe, S. D. Dabhi and P. K. Jha, A new flatland buddy as toxic gas scavenger: A first principles study, *J. Hazard. Mater.*, 2018, **351**, 337–345.
84 F. Schulz, R. Drost, S. K. Hämäläinen, T. Demonchaux, A. P. Seitsonen and P. Liljeroth, Epitaxial hexagonal boron nitride on Ir(111): A work function template, *Phys. Rev. B*, 2014, **89**, 235429–235437.

View Article Online
DOI: 10.1039/C8TB01649F

Table of contents (TOC)

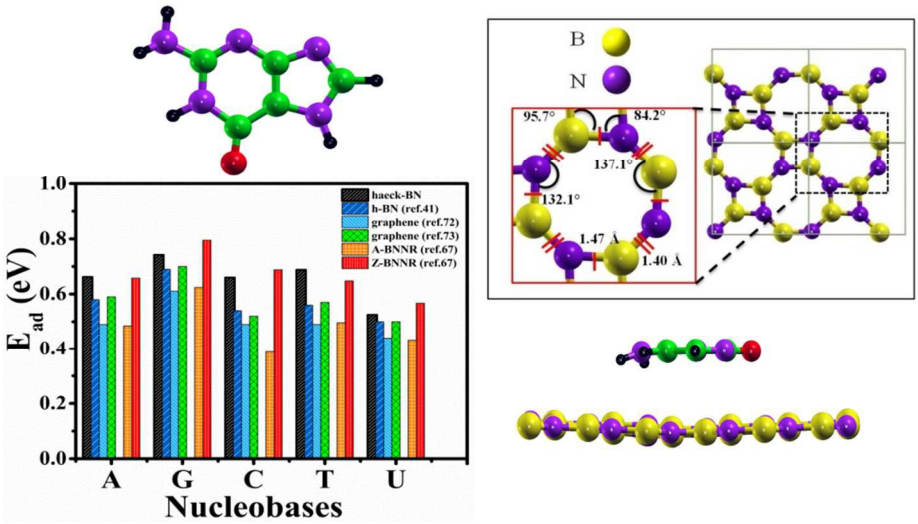

The study suggests that new Haeckelite structure of boron nitride may act as superior material with ultrafast recovery time for sensing and DNA sequencing application in future.